

UC Santa Cruz

UC Santa Cruz Previously Published Works

Title

The mIAA7 degron improves auxin-mediated degradation in *Caenorhabditiselegans*

Permalink

<https://escholarship.org/uc/item/3xk0g1j8>

Journal

G3: Genes, Genomes, Genetics, 12(10)

ISSN

2160-1836

Authors

Sepers, Jorian J
Verstappen, Noud HM
Vo, An A
et al.

Publication Date







2022-09-30

DOI

10.1093/g3journal/jkac222

Peer reviewed

The mIAA7 degron improves auxin-mediated degradation in *Caenorhabditis elegans*

Jorian J. Sepers ¹, Noud H.M. Verstappen ¹, An A. Vo,² James Matthew Ragle ², Suzan Ruijtenberg ¹, Jordan D. Ward ², Mike Boxem ^{1,*}

¹Division of Developmental Biology, Institute of Biodynamics and Biocomplexity, Department of Biology, Faculty of Science, Utrecht University, 3584 CH Utrecht, The Netherlands,

²Department of Molecular, Cell, and Developmental Biology, University of California-Santa Cruz, Santa Cruz, CA 95064, USA

*Corresponding author: Division of Developmental Biology, Institute of Biodynamics and Biocomplexity, Department of Biology, Faculty of Science, Utrecht University, Padualaan 8, 3584 CH Utrecht, The Netherlands. Email: m.boxem@uu.nl

Abstract

Auxin-inducible degradation is a powerful tool for the targeted degradation of proteins with spatiotemporal control. One limitation of the auxin-inducible degradation system is that not all proteins are degraded efficiently. Here, we demonstrate that an alternative degron sequence, termed mIAA7, improves the efficiency of degradation in *Caenorhabditis elegans*, as previously reported in human cells. We tested the depletion of a series of proteins with various subcellular localizations in different tissue types and found that the use of the mIAA7 degron resulted in faster depletion kinetics for 5 out of 6 proteins tested. The exception was the nuclear protein HIS-72, which was depleted with similar efficiency as with the conventional AID* degron sequence. The mIAA7 degron also increased the leaky degradation for 2 of the tested proteins. To overcome this problem, we combined the mIAA7 degron with the *C. elegans* AID2 system, which resulted in complete protein depletion without detectable leaky degradation. Finally, we show that the degradation of ERM-1, a highly stable protein that is challenging to deplete, could be improved further by using multiple mIAA7 degrons. Taken together, the mIAA7 degron further increases the power and applicability of the auxin-inducible degradation system. To facilitate the generation of mIAA7-tagged proteins using CRISPR/Cas9 genome engineering, we generated a toolkit of plasmids for the generation of dsDNA repair templates by PCR.

Keywords: mIAA7; TIR1; AID system; protein degradation; *Caenorhabditis elegans*

Introduction

Perturbing the functioning of proteins is essential to decipher their biological roles and can be accomplished using a wide variety of approaches (Housden et al. 2017). The desire to investigate the functioning of proteins in specific cell or tissue types or at specific developmental stages has led to the development of several methods that offer spatial or temporal control over protein expression. In *Caenorhabditis elegans*, tissue-specific RNA interference (RNAi) and conditional loss-of-function alleles utilizing targeted nucleases or recombinase strategies can conditionally interfere with protein functioning at the level of the corresponding mRNA or genetic locus (Hoier et al. 2000; Qadota et al. 2007; Davis et al. 2008; Cheng et al. 2013; Shen et al. 2014; Ruijtenberg and van den Heuvel 2015; Muñoz-Jiménez et al. 2017). To target proteins directly, several conditional protein depletion systems have been developed that mark proteins of interest for degradation by the 26S proteasome through ubiquitination (Cho et al. 2013; Armenti et al. 2014; Wang et al. 2017; Wu et al. 2017). The best-known of these systems are the ZF1-mediated degradation, nanobody-mediated degradation, and auxin-inducible degradation (AID) systems. ZF1-mediated degradation and nanobody-mediated degradation repurpose the endogenous E3 ubiquitin ligase substrate-recognition subunit ZIF-1 (Armenti et al. 2014;

Wang et al. 2017). The ZF1-mediated degradation system targets proteins that are tagged with the ZF1 zinc-finger domain by ectopic expression of ZIF-1 and can be combined with a *zif-1* loss-of-function background to avoid undesired degradation from endogenously expressed ZIF-1 (Armenti et al. 2014; Sallee et al. 2021). Nanobody-mediated degradation targets proteins that are tagged with a fluorescent protein by exogenously expressing ZIF-1 fused to a nanobody that targets the fluorescent protein (Wang et al. 2017). Finally, in the AID system, a protein of interest is tagged with an AID degron sequence derived from indole-3-acetic acid (IAA) proteins and combined with the expression of the plant-derived F-box protein transport inhibitor response 1 (TIR1) (Nishimura et al. 2009; Zhang et al. 2015). TIR1 forms a functional SKP-1-Cullin-F-box protein (SCF) E3 ubiquitin ligase complex with endogenous SCF proteins. In the presence of auxin (IAA), TIR1 associates with the AID degron resulting in polyubiquitination of the target protein (Nishimura et al. 2009; Zhang et al. 2015).

Most of the systems described above allow for spatial or temporal control, but not both simultaneously, by placing components of the system under control of tissue-specific or -inducible promoters. Combined spatial and temporal control could, however, be accomplished by incorporating bipartite expression systems (Nance and Frøkjær-Jensen 2019). In contrast, in the AID

Received: June 1, 2022. Accepted: August 15, 2022

© The Author(s) 2022. Published by Oxford University Press on behalf of Genetics Society of America.

This is an Open Access article distributed under the terms of the Creative Commons Attribution License (<https://creativecommons.org/licenses/by/4.0/>), which permits unrestricted reuse, distribution, and reproduction in any medium, provided the original work is properly cited.

system, expression of TIR1 from tissue-specific promoters confers spatial control while timing the addition of auxin offers temporal control over protein degradation.

The AID system has rapidly gained in popularity within the *C. elegans* community and various resources to facilitate its usage have been generated. For example, several strains are available that express TIR1 from different tissue-specific promoters (e.g. Zhang et al. 2015; Ashley et al. 2021) and cloning vectors are available that facilitate the generation of repair templates for genome editing (Ashley et al. 2021; Kroll et al. 2021; Negishi et al. 2022). Several improvements or alterations to the AID system have also been generated. These include synthetic auxin analogs that may cause less cytotoxicity or are more soluble in aqueous buffers (Martinez et al. 2020), and an auxin modification that is more effective at promoting protein degradation in embryos, presumably by better permeating the eggshell (Negishi et al. 2019).

Most recently, an improved AID system (AID2) was adapted for *C. elegans* that addresses 2 caveats of AID: leaky degradation that is observed for a subset of proteins and impact on the physiology of *C. elegans* caused by exposure to auxin (Yesbolatova et al. 2020; Hills-Muckey et al. 2022; Negishi et al. 2022). Ideally, auxin-induced protein degradation should occur strictly upon the addition of auxin, and the addition of auxin should not cause effects other than the degradation of the target protein. However, the AID system does suffer from leaky or basal degradation of at least a subset of target proteins in the absence of auxin, which can result in undesired phenotypes (Natsume et al. 2016; Li et al. 2019; Mendoza-Ochoa et al. 2019; Sathyan et al. 2019; Yesbolatova et al. 2019; Martinez et al. 2020; Schiksnis et al. 2020; Yesbolatova et al. 2020; Hills-Muckey et al. 2022; Negishi et al. 2022). In addition, the millimolar concentrations of auxin needed for maximum degradation efficacy increase the lifespan of worms and activate unfolded protein response pathways resulting in an enhanced protection against ER stress (Bhoi et al. 2021; Loose and Ghazi 2021; Hills-Muckey et al. 2022). The improved AID2 system relies on a TIR1 mutation (F79G in *Arabidopsis* TIR1) that alters the auxin-binding interface to fit the bulky auxin-derivative 5-phenyl-indole-3-acetic acid (5-Ph-IAA) (Hills-Muckey et al. 2022; Negishi et al. 2022). The use of this TIR1 variant greatly reduces leaky degradation while requiring low micromolar concentrations of 5-Ph-IAA that are less likely to affect the physiology of exposed animals.

One caveat of the AID system that has not yet been addressed in *C. elegans* is that some target proteins demonstrate slow degradation kinetics, incomplete depletion, or both, complicating their functional analysis (Patel and Hobert 2017; Serrano-Saiz et al. 2018; Duong et al. 2020; Riga et al. 2021). Here, we adapt an alternative AID degron sequence (mIAA7) that was shown to result in faster and more complete protein degradation in cultured human cells for use in *C. elegans* (Li et al. 2019). We show that the mIAA7 degron improves degradation for a panel of proteins with different subcellular locations, expressed across different tissues. While the mIAA7 degron did enhance the leaky degradation of 2 out of 4 proteins tested, we show that it can be effectively combined with the *C. elegans* AID2 system (*C.e.*AID2) to achieve more complete protein depletion without detectable leaky degradation. Finally, we demonstrate that using 2 or more degrons could improve degradation of ERM-1, the most challenging protein to degrade that we have encountered to date. Thus, the mIAA7 degron further expands the usefulness of the AID system to determine the biological functioning of proteins in *C. elegans*.

Methods

C. elegans strains and culture conditions

C. elegans strains were cultured under standard conditions (Brenner 1974). Only hermaphrodites were used. All experiments were performed with animals grown at 15°C or 20°C on standard Nematode Growth Medium (NGM) agar plates seeded with OP50 *Escherichia coli*. The HIS-72 timecourse experiment was performed in liquid culture (see below). Table 1 contains a list of all the strains used and their source.

Cloning of the mIAA7 repair template plasmids

The mIAA7 repair templates were cloned into pBSK+ (Addgene # 212207) using the Gibson assembly cloning strategy (Gibson et al. 2009). Linear DNA molecules were generated by PCR using Q5 polymerase (NEB) using primers (IDT) containing overhangs with the appropriate Gibson assembly sequences and, if applicable, the 12-amino acid glycine-rich linker. The mIAA7 sequence, based on Li et al. (2019), was codon-optimized for *C. elegans* with a synthetic intron and ordered as a gBlock Gene Fragment (IDT). The pJJS001–pJJS004 plasmids were assembled by inserting the mIAA7 and GFP or mCherry sequences directly into pBSK+. The pJJS005–pJJS012 plasmids were assembled by substituting the GFP of pJJS001 and pJJS002 plasmids with the respective fluorescent protein sequences. All assembly products were verified by Sanger sequencing (Macrogen Europe). pJW2341 was assembled by Gibson cloning a mIAA7 fragment into pJW2086 (Ashley et al. 2021). Cloning details are available upon request. Table 2 contains a list of all plasmids made with the respective primer sequences and origin of the fluorescent protein sequence, and full DNA sequences of all plasmids are provided in Supplementary File 1.

CRISPR/Cas9 genome editing

All alleles were made using the homology-directed repair of the CRISPR-Cas9-induced DNA double-strand breaks. Repair templates included, when appropriate, silent mutations to prevent recutting of repaired loci by Cas9. To verify the edits, the insertion sites were PCR amplified and sequenced by Sanger sequencing. Table 3 contains a list of all CRISPR-Cas9 edits made with the respective primer sequences, and Supplementary File 1 contains all final genomic sequences.

The *sax-7::AID*::GFP* allele was made using plasmid based expression of Cas9 and sgRNA and a plasmid repair template contain a self-excising cassette for selection of candidate integrants (Dickinson et al. 2015). Repair template and sgRNA plasmid were designed and assembled using the SapTrap cloning strategy (Dickinson et al. 2015; Schwartz and Jorgensen 2016). Reagents were injected and knock-in animals were recovered as previously described.

All other alleles were generated using microinjected Cas9 ribonucleoprotein complexes and linear repair templates, similar to the approach described by (Ghanta et al. 2021). We used a Cas9 amount of 250–700 ng/μl, a Cas9/crRNA ratio of 3.0–4.5, and a pSEM229 (*Pmlc-1::mNeonGreen*) or pRF4 (*rol-6(su1006)*) coinjection marker (Mello et al. 1991; El Mouridi et al. 2020). For tagging endogenous loci with a single AID* or mIAA7 degron and fluorescent protein, dsDNA repair templates were amplified using primers with 5' SP9 modifications (IDT) from the pJRK86 plasmid (AID*::GFP, Addgene # 173743) and mIAA7 repair template plasmids in Table 1. For *his-72* editing, GFP::AID*::3xFLAG repair templates were generated by PCR using a pJW2086 template and GFP::mIAA7::3xFLAG repair templates were generated by PCR

Table 1. List of strains used.

Strain	Genotype	Source
Bristol N2	Wild type	CGC
PD1074	Wild type	CGC
BOX246	<i>par-6(mib30[par-6::AID*::GFP-LoxP]) I</i>	Castiglioni et al. (2020)
BOX273	<i>mibIs48[Pelt-2::TIR1::tagBFP2-Lox511::tbb-2-3'UTR, IV:5014740-5014802 (cxTi10816 site)] IV</i>	Castiglioni et al. (2020)
BOX408	<i>mibIs49[Pwrt-2::TIR1::tagBFP2-Lox511::tbb-2-3'UTR, IV:5014740-5014802 (cxTi10816 site)] IV</i>	Castiglioni et al. (2020)
BOX409	<i>par-6(mib30[par-6::aid::GFP-loxp]) I; mibIs49[Pwrt-2::TIR1::tagBFP2-Lox511::tbb-2-3'UTR, IV:5014740-5014802 (cxTi10816 site)] IV</i>	Castiglioni et al. (2020)
BOX523	<i>ieSi57 [Peft-3::TIR1::mRuby::unc-54 3'UTR + Cbr-unc-119(+)] II; sax-7(mib45[sax-7::AID*::GFP])</i>	This study
BOX526	<i>mibIs48[Pelt-2::TIR1::tagBFP2-Lox511::tbb-2-3'UTR, IV:5014740-5014802 (cxTi10816 site)] IV; dlq-1(mib35[dlq-1::AID*::GFP-LoxP]) X</i>	Riga et al. (2021)
BOX623	<i>bbln-1(mib111[GFP::AID*::bbln-1]) X</i>	Remmelzwaal et al. (2021)
BOX632	<i>mibIs48[Pelt-2::TIR1::tagBFP2-Lox511::tbb-2-3'UTR, IV:5014740-5014802 (cxTi10816 site)] IV; bbln-1(mib111[GFP::AID*::bbln-1]) X</i>	Remmelzwaal et al. (2021)
BOX784	<i>mibIs48[Pelt-2::TIR1::tagBFP2-Lox511::tbb-2-3'UTR, IV:5014740-5014802 (cxTi10816 site)] IV; dlq-1(mib152[dlq-1::mIAA7::GFP]) X</i>	This study
BOX817	<i>mibIs48[Pelt-2::TIR1::tagBFP2-Lox511::tbb-2-3'UTR, IV:5014740-5014802 (cxTi10816 site)] IV; bbln-1(mib171[GFP::mIAA7::bbln-1]) X</i>	This study
BOX822	<i>bbln-1(mib172[GFP::mIAA7::bbln-1]) X</i>	This study
BOX823	<i>par-6(mib173[par-6::mIAA7::GFP]) I; mibIs49[Pwrt-2::TIR1::tagBFP2-Lox511::tbb-2-3'UTR, IV:5014740-5014802 (cxTi10816 site)] IV</i>	This study
BOX829	<i>par-6(mib174[par-6::mIAA7::GFP]) I</i>	This study
BOX838	<i>ieSi57 [Peft-3::TIR1::mRuby::unc-54 3'UTR + Cbr-unc-119(+)] II</i>	Zhang et al. (2015)
BOX847	<i>ieSi57 [Peft-3::TIR1::mRuby::unc-54 3'UTR + Cbr-unc-119(+)] II; sax-7(mib185[sax-7::mIAA7::GFP]) IV</i>	This study
BOX856	<i>sax-7(mib185[sax-7::mIAA7::GFP]) IV</i>	This study
BOX857	<i>sax-7(mib45[sax-7::AID*::GFP-loxP]) IV</i>	This study
BOX871	<i>erm-1(mib40[erm-1::mCherry::AID*]) I; mibIs50[Pelt-2::TIR1[F79G]::tagBFP2-Lox511::tbb-2-3'UTR, IV:5014740-5014802 (cxTi10816 site) *mibIs48] IV</i>	Remmelzwaal et al. (2021) and this study
BOX872	<i>erm-1(mib153[erm-1::mCherry::mIAA7]) I; mibIs51[Pelt-2::TIR1[F79G]::tagBFP2-Lox511::tbb-2-3'UTR, IV:5014740-5014802 (cxTi10816 site) *mibIs48] IV</i>	This study
BOX873	<i>erm-1(mib175[erm-1::mIAA7::mCherry::mIAA7]) I; mibIs52[Pelt-2::TIR1[F79G]::tagBFP2-Lox511::tbb-2-3'UTR, IV:5014740-5014802 (cxTi10816 site) *mibIs48] IV</i>	This study
BOX874	<i>erm-1(mib184[erm-1::mCherry::3x-mIAA7]) I; mibIs53[Pelt-2::TIR1[F79G]::tagBFP2-Lox511::tbb-2-3'UTR, IV:5014740-5014802 (cxTi10816 site) *mibIs48] IV</i>	This study
BOX875	<i>mibIs54[Peft-3::TIR1[F79G]::mRuby::unc-54 3'UTR + Cbr-unc-119(+)] *ieSi57] II; sax-7(mib185[sax-7::mIAA7::GFP]) IV</i>	This study
BOX879	<i>erm-1(mib187[erm-1::mCherry::2x-mIAA7]) I; mibIs56[Pelt-2::TIR1[F79G]::tagBFP2-Lox511::tbb-2-3'UTR, IV:5014740-5014802 (cxTi10816 site) *mibIs48] IV</i>	This study
BOX880	<i>erm-1(mib191[erm-1::mIAA7::mCherry::]) I; mibIs57[Pelt-2::TIR1[F79G]::tagBFP2-Lox511::tbb-2-3'UTR, IV:5014740-5014802 (cxTi10816 site) *mibIs48] IV</i>	This study
BOX882	<i>par-6(mib173[par-6::mIAA7::GFP]) I; mibIs58[Pwrt-2::TIR1[F79G]::tagBFP2-Lox511::tbb-2-3'UTR, IV:5014740-5014802 (cxTi10816 site) *mibIs49] IV</i>	This study
SUR5	<i>rubSi4[rps-26::AID*::GFP]</i>	This study
SUR23	<i>rubSi4[rps-26::AID*::GFP]; Pmyo-3::TIR1::mRuby</i>	This study
SUR31	<i>rubSi10[rps-26::mIAA7::GFP]</i>	This study
SUR32	<i>rubSi11[rps-26::mIAA7::GFP]; Pmyo-3::TIR1::mRuby</i>	This study
IFM160	<i>bchSi59[Pmyo-3::TIR1::mRuby::tbb-2utr]II</i>	Venz et al. (2021)
JDW225	<i>wdSi23[Peft-3::TIR1::F2A::mTagBFP2::AID*::NLS::tbb-2 3'UTR, I:-5.32]</i>	Ashley et al. (2021)
JDW430	<i>wdSi23[Peft-3::TIR1::F2A::mTagBFP2::AID*::NLS::tbb-2 3'UTR, I:-5.32] I; his-72(wrd100[GFP::AID*::3xFLAG::his-72]) III</i>	This study
JDW431	<i>wdSi23[Peft-3::TIR1::F2A::mTagBFP2::AID*::NLS::tbb-2 3'UTR, I:-5.32] I; his-72(wrd101[GFP::mIAA7::3xFLAG::his-72]) III</i>	This study

using a pJW2341 repair template (Table 1). For tagging ERM-1 with 2 degrons, a second mIAA7 degron was inserted into the existing ERM-1::mCherry::mIAA7 allele using similar dsDNA repair templates amplified from an mIAA7 repair template plasmids in Table 1. The C-term 3× ERM-1 allele was generated using the same reagents as the C-term 2× allele but was the result of a fortuitous incorrect repair event. The TIR1[F79G] alleles were generated using a ssDNA oligo repair template (IDT).

Auxin treatment of synchronized worms

Animals were developmentally synchronized by hypochlorite bleaching of gravid adults to release embryos, which were hatched overnight in M9 buffer. For HIS-72, depletion experiments

were performed in liquid culture. Approximately 14,000 synchronized L1 animals were resuspended in 6 ml of M9 + 0.025% gelatin supplemented with 13.3% (v/v) concentrated OP50 and either 4% ethanol (control) or 4 mM IAA (or auxin) in ethanol. All other depletion experiments were performed on agar plates. Synchronized L1 larvae were first placed on NGM plates seeded with *E. coli* OP50 and allowed to develop for 24–48 h. Animals were then transferred to NGM plates seeded with *E. coli* OP50 and containing 1 mM, 50 μM, or 5 μM IAA, or 1 μM 5-Ph-IAA. Auxin NGM plates were prepared by diluting 1M IAA (Alfa Aesar) or 1 mM 5-Ph-IAA (BioAcademia) dissolved in 100% ethanol into NGM agar that was cooled down to ~50°C prior to plate pouring.

Table 2. Primer sequences for plasmids.

pJJS001 pBSK For. pBSK Rev. mIAA7 For. mIAA7 Rev. GFP For. GFP Rev.	mIAA7::GFP::Linker TGGCAGTGGAGGTACCGGCGGAAGCGGTGCGGTGGAGCTCCAGCTTTTGTTC CCAAATTCGCCCTATAGTGAGTCG CTCACTATAGGGCGAATTGGATGGGATTCTCCGAGACC CCTTGGACATGGAGGAGGTCTTTTGTG GACCTCCTCCATGTCCAAGGGAGAGGAAC CGCCGGTACCTCCACTGCCACCGCTGCCCTTGTAGAGCTCGTCCATTC	GFP origin: pJIR82 (Addgene # 75027)
pJJS002 pBSK For. pBSK Rev. mIAA7 For. mIAA7 Rev. GFP For. GFP Rev.	Linker::GFP::mIAA7 GCGGTGGAGCTCCAGCTTTTGTTC CGCCGGTACCTCCACTGCCACCGCTGCCCAATTCCGCCCTATAGTGAGTCCG GCTCTACAAGGGATTCTCCGAGACCGTC AAAAGCTGGAGCTCCACCGCGGAGGAGGTCTTTTGTG TGGCAGTGGAGGTACCGGCGGAAGCGGTATGTCCAAGGGAGAGGAAC CGGAGAATCCCTTGTAGAGCTCGTCCATTCCGTGG	
pJJS003 pBSK For. pBSK Rev. mIAA7 For. mIAA7 Rev. mCherry For. mCherry Rev.	mIAA7::mCherry::Linker TGGCAGTGGAGGTACCGGCGGAAGCGGTGCGGTGGAGCTCCAGCTTTTGTTC CCAAATTCGCCCTATAGTGAGTCG CTCACTATAGGGCGAATTGGATGGGATTCTCCGAGACC CCTTGGACATGGAGGAGGTCTTTTGTG GACCTCCTCCATGTCCAAGGGAGAGGAGACAAC CGCCGGTACCTCCACTGCCACCGCTGCCCTTGTAGAGCTCGTCCATTC	mCherry origin: pJIR83 (Addgene # 75028)
pJJS004 pBSK For. pBSK Rev. mIAA7 For. mIAA7 Rev. mCherry For. mCherry Rev.	Linker::mCherry::mIAA7 GCGGTGGAGCTCCAGCTTTTGTTC CCAAATTCGCCCTATAGTGAGTCG GCTCTACAAGGGATTCTCCGAGACCGTC AAAAGCTGGAGCTCCACCGCGGAGGAGGTCTTTTGTG CTCACTATAGGGCGAATTGGGGCAGCGGTGGCAGTGGGA CGGAGAATCCCTTGTAGAGCTCGTCCATTCCCTCCG	
pJJS005 pJJS001 For. pJJS001 Rev. mNG For. mNG Rev.	mIAA7::mNG::Linker GCTCTACAAGGGCAGCGGTGGCAGT TGGAGACCATGGAGGAGGTCTTTTGTGGG GACCTCCTCCATGGTCTCCAAGGGAGAGG CACCGCTGCCCTTGTAGAGCTCGTCCATTCCC	mNG origin: pDD346 (Addgene # 133311)
pJJS006 pJJS002 For. pJJS002 Rev. mNG For. mNG Rev.	Linker::mNG::mIAA7 GCTCTACAAGGGATTCTCCGAGACCGTC TGGAGACCATACCGCTTCCGCCGGTA CGGAAGCGGTATGGTCTCCAAGGGAGAGGAG CGGAGAATCCCTTGTAGAGCTCGTCCATTCC	
pJJS007 pJJS001 For. pJJS001 Rev. mScarlet For. mScarlet Rev.	mIAA7::wrmScarlet::Linker GCTCTACAAGGGCAGCGGTGGCAGT TGCTGACCATGGAGGAGGTCTTTTGTGGG GACCTCCTCCATGGTCAAGGGAGAGG CACCGCTGCCCTTGTAGAGCTCGTCCATTCC	wrmScarlet origin: Codon optimized gBlock
pJJS008 pJJS002 For. pJJS002 Rev. mScarlet For. mScarlet Rev.	Linker::wrmScarlet::mIAA7 GCTCTACAAGGGATTCTCCGAGACCGTC TGCTGACCATACCGCTTCCGCCGGTA CGGAAGCGGTATGGTCAAGGGAGAGG CGGAGAATCCCTTGTAGAGCTCGTCCATTCCCTC	
pJJS009 pJJS001 For. pJJS001 Rev. mKate2 For. mKate2 Rev.	mIAA7::mKate2::Linker ACACCGTAAGGGCAGCGGTGGCAGT CGGAGACCATGGAGGAGGTCTTTTGTGGG GACCTCCTCCATGGTCTCCGAGCTCATTAAAGAA CACCGCTGCCCTTACGGTGTCCGAGCTTG	mKate2 origin: pDD375 (Addgene # 91825)
pJJS010 pJJS002 For. pJJS002 Rev. mKate2 For. mKate2 Rev.	Linker::mKate2::mIAA7 ACACCGTAAGGGATTCTCCGAGACCGTC CGGAGACCATACCGCTTCCGCCGGTA CGGAAGCGGTATGGTCTCCGAGCTCATTAAAGA CGGAGAATCCCTTACGGTGTCCGAGCTTG	
pJJS011 pJJS001 For. pJJS001 Rev. mTagBFP2 For. mTagBFP2 Rev.	mIAA7::mTagBFP2::Linker CAAGCTCAACGGCAGCGGTGGCAGT CGGAAACCATGGAGGAGGTCTTTTGTGGG GACCTCCTCCATGGTTCGGAAATTGATTAAGGAA CACCGCTGCCCTTGTAGCTTGTGTCCGAGC	TagBFP2 origin: JDW233 (Ashley et al. 2021)
pJJS012 pJJS002 For. pJJS002 Rev. mTagBFP2 For. mTagBFP2 Rev.	Linker::mTagBFP2::mIAA7 CAAGCTCAACGGATTCTCCGAGACCGTC CGGAAACCATACCGCTTCCGCCGGTA CGGAAGCGGTATGGTTTCCGAATTGATTAAGGAA CGGAGAATCCCTTGTAGCTTGTGTCCGAGC	
pJW2341 pJW2086 For. pJW2086 Rev. mIAA7 For. mIAA7 Rev.	Linker::GFP::mIAA7::3xFLAG::Linker GAGCATGAGGTGCGACGGTCTCGGAGAATCCCCGCCACCTCCGGATCCGGATTGAAAG AACATGATGACCCAACAAAAGACCTCCTCCGGTGGTGGCGTTCTGGCTCAGG GGATTCTCCGAGACCGTCGACCTC GGAGGAGGTCTTTTGTGGGTGCATC	

Table 3. Genome engineering reagents.

dlg-1::mIAA7::GFP	
crRNA	GCCACGTCATTAGATGAAAT
Repair template For.	GTGAATCGCAGACGCCAATTTGGGTGCCACGTCATGGATTCTCCGAGACCGT
Repair template Rev.	GAGACAATTGAGAATATTGTTTAAAAAATAAAAAGAAAATACGATAGAACAAATAATTAGGAGGAGGTCTTT-TGTTGGG
Genotyping For.	AGTGGCGAAGAAGCTCAAGC
Genotyping Rev.	CCACAATCACTGCCAGAAAACGG
par-6::mIAA7::GFP	
crRNA	AAATGATTCGGACAGTGGAG
Repair template For.	TCCGAAACAGCACGACGCAAATGATTCCGACAGTGGAGAAGACGGATTCTCCGAGACCGT
Repair template Rev.	AAAATCGAGGAAAAATGGTGAAAAGAGTTTTTCACTTGTAGAGCTCGTCCATTC
Genotyping For.	ACGAGGACCGTCACAACAAG
Genotyping Rev.	AGTATGGGCTCAGAGAGCTCTG
GFP::mIAA7::bbln-1	
crRNA	CTCATTTTCAGTTGAACACAA
Repair template For.	TCTTTTCTCCATTTCCCTCATTTTCAGTTGAACACAATGTCCAAGGGAGAGGAAAC
Repair template Rev.	ACAATAGGCTCTTGTCTTTCTGCTCAACGACCATGGAGGAGGTCTTTTGTGG
Genotyping For.	ATCATCACCATCATCATCACC
Genotyping Rev.	GTCACTTCTCCTTGGTTGAG
rps-26::AID*::GFP	
crRNA	GAACAAACAACCTTATGGAGC
Repair template For.	CTGCTGCTCGTCCAGGAGCTCCAGGACCACGTCCAATGCCTAAAGATCCAGCCAA
Repair template Rev.	AAAAAGGTTTATAATTTCAAAGAACAACAACCTTAGTAGAGCTCGTCCATTCCGT
Genotyping For.	ATCCACAGCAAGGTCGTCAAG
Genotyping Rev.	GAGCAACACAATTCAGTTCGGG
rps-26::mIAA7::GFP—same genotyping primers as rps-26::AID*::GFP	
crRNA	GAACAAACAACCTTATGGAGC
Repair template For.	CCGCTGCTGCTCGTCCAGGAGCTCCAGGACCACGTCCAATGGGATTCTCCGAGACCGTC
Repair template Rev.	AAAAAGGTTTATAATTTCAAAGAACAACAACCTTAGTAGAGCTCGTCCATTCCGTG
sax-7::AID*::GFP^a	
sgRNA 1 For.	TTGCCGGCCGAACGGCCCGAGAA
sgRNA 1 Rev.	AACTTCTCGGGCCGTTTCGGCCGG
sgRNA 2 For.	TCTTCCGGCCGAACGGCCCGAGAA
sgRNA 2 Rev.	AACTTCTCGGGCCGTTTCGGCCGG
sgRNA 3 For.	TCTTGTCCACAAAAGAGCTTGATGC
sgRNA 3 Rev.	AAACGCATCAAGCTTTTTGTGGAC
Left homology arm For.	CTGCTTTCGTGGCTATCCAGTATCACAGCGTGAGCC
Left homology arm Rev.	GTGCTCTTCGCGCGACAAACGTGACGTTGATCCTTTTTCTGGACGCTCGGCTG
Right homology arm For.	CTGCTTTCGACGTAGAAGACTATCCACGTGTTCCCTC
Right homology arm Rev.	GTGCTCTTCGTACGTCCTACCCACATGGTTATCCG
Genotyping For.	GCCACAAGATGCTGATGAATGG
Genotyping Rev.	GGTAAAAGCTCTGGCAAACGTC
sax-7::mIAA7::GFP	
crRNA	GTCGACGTTGATCCTTTCTC
Repair template For.	TCTTTTCTCCATTTCCCTCATTTTCAGTTGAACACAATGTCCAAGGGAGAGGAAAC
Repair template Rev.	ACAATAGGCTCTTGTCTTTCTGCTCAACGACCATGGAGGAGGTCTTTTGTGG
Genotyping For.	ATCATCACCATCATCATCACC
Genotyping Rev.	GTCACTTCTCCTTGGTTGAG
GFP::AID*::3xFLAG::his-72 and GFP::mIAA7::3xFLAG::his-72	
crRNA	GGTACGAGCCATTGTTGTTT
Repair template For.	TCCAACCATTCTCAATTCTCAATTTCCAGAACAACAATGAGTAAAGGAGAAGAATTGTTCACTGG
Repair template Rev.	CCGGTGGATTTACGAGCGGTTTGCTTGGTACGAGCTGAGGCTCCCGATGCTCCCTTG
Genotyping For.	CGATCGATAGTGACACGCGA
Genotyping Rev.	CACAGGTTGGTGTCTCGAA
TIR1[F79G]	
crRNA	AGGTTGAAGTCGGCGAAGTG
Repair template	AAGGTCGTTCCGTCGAGCTCAAGGGAAAGCCACATGGAGCCGATTTCAATCTTGTCCAGACGGATGGGA-GGATACGTCTACCCATG
Genotyping For.	AGAAGAAGTACTCGAGCAGC
Genotyping WT Rev.	AGGTTGAAGTCGGCGAAG
Genotyping F79G Rev.	GACAAGATTGAAATCGGCTCC
Sequence Rev.	TTGAGCTTGAGGGACTTGAG
erm-1::mCherry::mIAA7	
crRNA	ATATTGTTTAAAAAATAAA
Repair template For.	ACACAAAACGAAGAATCGATCAATACGAAAATATGGGCAGCGGTGGCAGTGGAA
Repair template Rev.	GAGACAATTGAGAATATTGTTTAAAAAATAAAAAGAAAATACGATAGAACAAATAATTAGGAGGAGGTCTT-TTGTGGG
Genotyping For.	AACTCGGTATTTCCCTTACG
Genotyping Rev.	ATTGTTAAAAGGCACTGATGG
erm-1::mCherry::2x-mIAA7—same genotyping primers as erm-1::mCherry::mIAA7	
crRNA	AGGAATGGAGGAGCTCTACA
Repair template For.	GGGACGTCACCTCCACGGAGGAAATGGACGAGCTCTACAAAGGATTCTCCGAGACCGT
Repair template Rev.	AGGTTGAGCATGAGGTCGACGGTCTCGGAGAAATCCGGAGGAGGTCTTTTGTGG

(continued)

Table 3. (continued)

<i>erm-1::mIAA7::mCherry</i>—same genotyping primers as <i>erm-1::mCherry:mIAA7</i>	
crRNA 1	ATATTGTTTAAAAAATAAA
crRNA 2	AAGACTCTCCGTCAAATCCG
Repair template For. 1	TTGAGACAAATTCGCGGAGGAAACACGAAGAGGCGCATCGACCAATACGAGAACATGGGATTCTCCGAGACC-GT
Repair template For. 2	AGAACAAAAAGCCGGACGCGACAAGTACAAGACTTTGAGACAAATTCGCGGAGG
Repair template Rev.	AGACAATTGAGAATATTGTTTAAAAAATAAAAGTAAATACGATAGAACAAATAATTACTTGTAGAGTCGT-CCATTC
<i>erm-1::mIAA7::mCherry::mIAA7</i>—same genotyping primers as <i>erm-1::mCherry:mIAA7</i>	
crRNA	AGCGGTGGCAGTGGAGGTAC
Repair template For.	AATACGAAAATATGGGCAGCGGTGGCAGTGGAGGTGGATTCTCCGAGACCGT
Repair template Rev.	TCCTCTCTCCCTTGACATACCGCTTCGCCGGTGGAGGAGTCTTTTGTGG

^a Three crRNAs were used since 1 was not efficient enough.

^b Two crRNAs were used since 1 was not efficient enough. In addition, due to a size limitation of the primer oligo, the repair template was generated using 2 PCRs. An initial PCR using “repair template For. 1,” and a second reaction using “Repair template For. 2” and the product of the first reaction as template.

Western blot analysis

At each timepoint, 500 μ l of animals in solution was removed (~1,160 larvae), and samples for western blotting were generated similar to [Vo et al. \(2021\)](#), except samples were resuspended in 100 μ l of M9 + 0.025% gelatin and freeze-cracked twice on dry ice before Laemmli sample buffer was added to 1 \times and samples were boiled for 5 min. Five microliters of lysate was resolved on precast 4–20% Mini-Protean TGX Stain Free Gels (Bio-Rad) before being transferred to a polyvinylidene difluoride membrane by semi-dry transfer with a TransBlot Turbo (Bio-Rad). Blots were probed with 1:2,000 horseradish peroxidase (HRP)-conjugated anti-FLAG M2 (Sigma-Aldrich, A8592-5x1MG, Lot # SLCB9703) or 1:2,000 mouse anti-alpha-Tubulin 12G10 concentrated supernatant (Developmental Studies Hybridoma Bank). For the anti-alpha tubulin blot, we used 1:10,000 Digital anti-mouse HRP conjugate (Kindle Biosciences LLC, R1005) secondary antibody. Blots were developed similar to [Johnson et al. \(2021\)](#) using Supersignal West Femto Maximum Sensitivity Substrate (Thermo Fisher Scientific, 34095) and the high-resolution setting on a ChemiDoc MP system (Bio-Rad).

Epifluorescence microscopy

At each HIS-72 depletion, timepoint images were collected by removing 100 μ l of culture of the indicated genotype and treatment, adding 1 ml of M9 + 0.025% gelatin, pelleting at 700g, washing twice in M9 + 0.025% gelatin, and then transferring animals to a 2% agarose pad. Ten microliters of 5 mM levamisole was added to immobilize animals and a cover slip was placed on top. Images were acquired on an AxioImager M2 microscope (Carl Zeiss Microscopy, LLC) equipped with a Colibri 7 LED light source and an AxioCam 506 mono camera using a Plan-Apochromat 63x/1.40 Oil DIC lens. Acquired images were processed through Fiji software version: 2.3.0/1.53q ([Schindelin et al. 2012](#)).

Spinning disk confocal microscopy

Larvae were mounted on a 5% agarose pad in 20 mM tetramisole solution in M9 to induce paralysis. Spinning disk confocal imaging was performed using a Nikon Ti-U microscope equipped with a Yokogawa CSU-X1 spinning disk using a 60 \times -1.4 NA objective, 488- and 561-nm lasers, Semrock “530” GFP-L and “600” TxRed emission filters, and an Andor iXON DU-885 camera. Spinning disk images were acquired using MetaMorph Microscopy Automation & Image Analysis Software. Image scales were calibrated using a micrometer slide. All stacks along the z-axis were obtained at 0.25- μ m intervals, and maximum intensity Z projections were done in Fiji software. For display in figures, level adjustments, false coloring, and image overlays were done in Adobe Photoshop. Image rotation, cropping, and panel assembly

were done in Adobe Illustrator. All edits were done nondestructively using adjustment layers and clipping masks, and images were kept in their original capture bit depth until final export from Illustrator for publication.

Quantitative image analysis

Quantitative analysis of spinning disk images was done in Fiji and Python. All measurement values were first corrected for imaging system background levels by subtracting the average of a region within the field of view that did not contain any animals. For the measurements of the intestinal apical junctions (DLG-1) and membrane (BBLN-1 and ERM-1), analyses were done on intestinal cells forming int2 through int6, at the center of the intestinal lumen. A maximum projection of 5 slices was made, and 3 25-px-wide line scans perpendicular to the apical junction or membrane were taken per animal. For the measurements of the cortex of the cell body of the ALM neuron (SAX-7), 2 10-px-wide line scans using a maximum projection of 3 slices were taken perpendicular to the membrane per animal. For each line scan, the peak value and cytoplasmic value were determined using the peak finding tools of the Scipy Signal Python datapack with `rel_height` of 1.0 ([Virtanen et al. 2020](#)). Cytoplasmic values were subtracted from the corresponding peak values, and the resulting final junctional or membrane intensity values were averaged per animal. For SAX-7, exposure to auxin of 3 h or longer resulted in complete depletion and an inability to locate the ALM cell body. For these timepoints, values were plotted at 0 and no statistics were performed. For the measurement of PAR-6 at the apical domain of the seam cells and RPS-26 in the body wall muscle cytoplasm, averages of 3 regions were determined using a max projection of 3 slices (PAR-6) or a single slice (RPS-26).

C. elegans growth curves

To measure growth curves, L1 animals synchronized as described above were placed on NGM plates seeded with *E. coli* OP50 prepared as described above. Images were taken at 24-h intervals up to 72 h, using a Zeiss Axio Imager 2 equipped with a \times 20-0.5 NA objective and AxioCam MRm CCD (charge-coupled device) monochrome camera, driven by Zen Pro software. Animal length was quantified in FIJI software by drawing a line along the center line of the animal.

Statistical analysis

All statistical analyses were performed using GraphPad Prism 8. For population comparisons, a D’Agostino and Pearson test of normality was first performed to determine if the data were sampled from a Gaussian distribution. For data drawn from a

Gaussian distribution, comparisons between 2 populations were done using an unpaired t-test, with Welch's correction if the SDs of the populations differ significantly, and comparisons between >2 populations were done using a 1-way ANOVA if the SDs of the populations differ significantly. For data not drawn from a Gaussian distribution, a nonparametric test was used (Mann-Whitney for 2 populations and Kruskal-Wallis for >2 populations). ANOVA and nonparametric tests were followed up with multiple comparison tests of significance (Dunnett's, Tukey's, Dunnett's T3, or Dunn's). Tests of significance used and sample sizes are indicated in the figure legends. No statistical method was used to predetermine sample sizes. No samples or animals were excluded from analysis. The experiments were not randomized, and the investigators were not blinded to allocation during experiments and outcome assessment. All presented graphs were made using GraphPad Prism and Adobe Illustrator. ns is $P > 0.05$, * is $P \leq 0.05$, ** is $P \leq 0.01$, *** is $P \leq 0.001$, and **** is $P \leq 0.0001$.

Results

The mIAA7 degron improves AID-mediated degradation

AID degrons are derived from IAA proteins and consist of the conserved domain required for TIR1 recognition (Domain II) and flanking sequences (Gray et al. 2001; Ramos et al. 2001). The two most commonly used degron sequences, termed AID* and mAID, are based on the IAA17 protein (Fig. 1a) (Kubota et al. 2013; Morawska and Ulrich 2013). An alternative degron sequence derived from IAA7 was recently shown to result in faster and more complete protein degradation in cultured human cells, compared to the mAID degron (Li et al. 2019). This degron, termed mIAA7, contains the IAA7 Domain II and includes a longer N-terminal flanking region than AID* or mAID (Fig. 1a).

To assess the effectiveness of the mIAA7 degron in *C. elegans*, we selected the Discs large ortholog DLG-1 as an initial test protein to degrade. DLG-1 is a cell polarity regulator that is involved in the formation of cell-cell junctions and is essential for embryonic development (Bossinger et al. 2001; Firestein and Rongo 2001; Köppen et al. 2001; McMahon et al. 2001). Previously, we found that the conventional AID* degron was ineffective at mediating the degradation of DLG-1 (Riga et al. 2021). To determine if use of the mIAA7 degron results in more effective degradation, we tagged the endogenous *dlg-1* locus with codon optimized mIAA7 and GFP sequences by homology-directed repair of CRISPR/Cas9-induced DNA double-strand breaks, using the same insertion site and tag order used previously to generate the *dlg-1::AID*::GFP* locus. We then compared the degradation kinetics of AID* and mIAA7 tagged DLG-1 in the intestine, using a single-copy integrated transgene expressing TIR1 from the intestine specific *elt-2* promoter. We exposed synchronized larvae to auxin from the L3 stage and quantified the levels of DLG-1 at apical junctions of intestinal cells at various timepoints over a 24-h time period. Consistent with our previous observations, depletion of DLG-1 tagged with AID* was inefficient, with junctional fluorescence levels similar to controls not exposed to auxin for the complete duration of the experiment (Fig. 1b). In contrast, DLG-1 tagged with mIAA7 was depleted to 4.8% of starting levels after 12 h of auxin exposure (Fig. 1b). Degradation was not fully complete, as low levels of DLG-1 remained detectable even after 24 h of exposure to auxin, particularly at the apical junctional sites where 3 intestinal cells meet (Fig. 1b). Nevertheless, the use of the mIAA7 degron dramatically improved the efficiency of auxin-mediated degradation of DLG-1 in *C. elegans*.

To evaluate the effectiveness of the mIAA7 degron more systematically, we next investigated the degradation kinetics of a variety of proteins using both AID* and mIAA7. The proteins were chosen to represent distinct subcellular localizations and their degradation was investigated in different tissue types. We investigated degradation of the apical polarity regulator PAR-6 in larval seam cells, of the intermediate filament regulator BBLN-1 in intestinal cells, of the adhesion protein SAX-7 in the ALM neurons, and of the ribosomal protein RPS-26 in body wall muscle cells. For SAX-7, measurements were taken in the ALM cell body, since degradation in neurites was ineffective in most if not all neurons. For each of these proteins, endogenous lines expressing the protein tagged with AID* and a fluorescent protein had previously been generated in our groups. We generated mIAA7-tagged variants keeping the tag order and orientation (N- or C-terminal) and introducing as few other changes to the protein amino acid sequence as possible (Supplementary File 1). We then performed timecourse experiments with synchronized animals to compare the degradation efficiencies, adding auxin at the L2- (PAR-6 and RPS-26) or L3 stage (BBLN-1 and SAX-7) and quantifying fluorescence levels at indicated intervals (Fig. 2). PAR-6 levels were measured at seam-hyp7 junctions, BBLN-1 levels at the apical intermediate filament layer, SAX-7 levels at the cell wall of the ALM cell body, and RPS-26 in the cytoplasm of body wall muscle cells. PAR-6, BBLN-1, and SAX-7 are already highly efficiently degraded using the AID* degron. For these proteins, we lowered the auxin concentration from 1 mM to 5 or 50 μ M to increase the time needed for degradation. Under these conditions, for each of these proteins, maximum depletion was achieved twice as fast with the mIAA7 degron compared to the AID* degron (Fig. 2a and Supplementary Fig. 1a). More strikingly, mIAA7-mediated degradation of the ribosomal protein RPS-26 in the body wall muscle cells resulted in complete degradation in 6 h compared to 24 h with the AID* degron (Fig. 2a and Supplementary Fig. 1a). Thus, for all 4 proteins, use of mIAA7 increases the degradation efficiency.

Finally, we tested the ability of the IAA7 degron to improve the degradation of the nuclear histone protein HIS-72, as several nuclear proteins showed only a modest increase in degradation efficiency with the mIAA7 degron in human cells (Li et al. 2019). We previously observed that the degradation efficiency of HIS-72 tagged with AID* varied between cell types, making this protein a good test case to detect a potential difference in degradation kinetics (our unpublished data). To be able to monitor HIS-72 levels in individual cells by immunofluorescence as well as measure overall HIS-72 levels by Western blot, we inserted sequences encoding GFP, the AID* or mIAA7 degron, and a triple FLAG tag at the start codon of the *his-72* locus. We exposed synchronized L1 animals ubiquitously expressing TIR1 to auxin and analyzed HIS-72 levels by fluorescence microscopy and Western blot analysis over a 6-h period at 2-h intervals. Control animals were not exposed to auxin. By Western blot analysis, HIS-72 levels were reduced but not absent after 2 h of exposure to auxin using both the AID* and mIAA7 degrons. HIS-72 levels did not decrease further upon prolonged auxin exposure and using either degron. These findings were corroborated by the fluorescence microscopy analysis. At 2 h of auxin exposure, HIS-72 levels in cells in the central region of the body were sharply reduced, while HIS-72 levels in cells in the head and tail regions appeared unaffected (Supplementary Fig. 2b). Further exposure to auxin up to 6 h did not appear to decrease HIS-72 levels in the head and tail regions. Thus, the mIAA7 degron does not appear to improve the

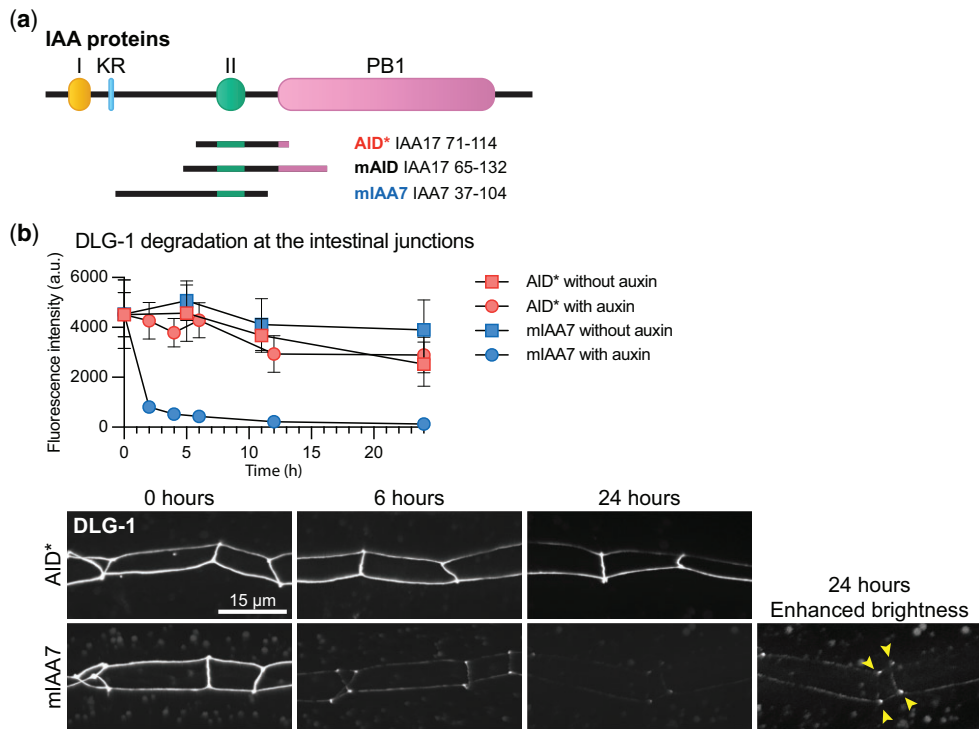


Fig. 1. The mIAA7 degron improves auxin-mediated degradation of DLG-1. a) Schematic overview of IAA proteins and the different AID degrons that have been derived from them. I = domain I; II = domain II; KR = conserved lysine and arginine residue; PB1 = Phox and Bem1p domain. b) Comparison between AID* and mIAA7-mediated degradation kinetics of intestinal DLG-1 in L3 larvae using 1 mM auxin. Values in the graph are arbitrary units and each data point represents the average intensity at intestinal cell junctions for the given condition and timepoint. Error bars: mean \pm SD; n: 7–20 animals. Images shown are representative maximum intensity projections that were acquired and displayed with the same settings for comparison, except for the indicated panel with enhanced brightness to show residual DLG-1. Arrowheads point to the apical junctional sites where 3 intestinal cells meet.

efficiency of HIS-72 depletion, but does function comparably to the AID* degron for this protein.

Improved protein degradation kinetics are ultimately expected to yield stronger loss-of-function phenotypes or a more rapid onset of phenotypes upon addition of auxin. To test this, we measured larval growth upon degradation of PAR-6 in the epidermis from hatching. We recently showed that full depletion of epidermal PAR-6 causes a severe growth defect, in which larvae do not grow beyond L1 size (Castiglioni et al. 2020). We therefore exposed animals to two auxin concentrations: a conventional 1 mM concentration that we had previously found to result in an incomplete growth arrest using the AID* degron, and the 5 μ M concentration used to quantify PAR-6 protein levels above. Animals with mIAA7-tagged PAR-6 on 1 mM auxin have a full growth arrest, while the other conditions resulted in a partial growth defect (Fig. 2c). Importantly, at both concentrations the growth defect was stronger for PAR-6 tagged with the mIAA7 degron than for AID*-tagged PAR-6, with the mIAA7 degron yielding a growth defect at 5 μ M that was very similar to that obtained with the IAA7 degron at 1 mM auxin (Fig. 2c). These results illustrate that the mIAA7 degron can induce stronger knockdown phenotypes that the AID* degron.

Taken together, our data demonstrate that the mIAA7 degron robustly increases the efficiency of AID-induced protein degradation across multiple tissues and cellular compartments, except for the nuclear protein HIS-72. The latter result might suggest that the degradation speed of nuclear proteins is mainly limited by the accessibility of TIR1 to the nuclear proteins rather than the degron sequence, though more nuclear proteins will need to be tested to assess the generalizability of this hypothesis.

However, this assertion is in line with mIAA7-mediated degradation data in human cells, where improved degradation of nuclear proteins was achieved by expressing TIR1 with a nuclear localization signal (NLS) sequence (Li et al. 2019).

mIAA7 can increase leaky degradation of target proteins

The increase in degradation efficiency conferred by the mIAA7 degron raises the possibility that leaky degradation levels are similarly increased. To investigate this possibility, we determined depletion levels of PAR-6, BBLN-1, SAX-7, and RPS-26 tagged with the AID* or mIAA7 degron as above in strains lacking or expressing TIR1. For RPS-26, we did not observe significant leaky degradation with either degron (Fig. 2d and Supplementary Fig. 2a). For BBLN-1, we observed moderate leaky degradation, with a ~17% decrease in fluorescence intensity using the AID* degron upon TIR1 expression in the intestine (Fig. 2d and Supplementary Fig. 2a). However, use of the mIAA7 degron did not increase the leaky degradation of BBLN-1 (Fig. 2d and Supplementary Fig. 2a). For PAR-6 and SAX-7, we observed more severe levels of leaky degradation that were significantly increased using the mIAA7 degron compared to the AID* degron. For PAR-6, leaky degradation was increased from 31% to 42% in the seam cells, and for SAX-7 leaky degradation increased from 45% to 72% in the ALM neuron cell body (Fig. 2d and Supplementary Fig. 2a). Despite these reduced protein levels, no overt phenotypes were observed for any of these proteins. Together, these data corroborate that for some target proteins leaky degradation is a potential caveat of the AID system. In addition, the use of a more effective degron, such as mIAA7, can increase leaky degradation.

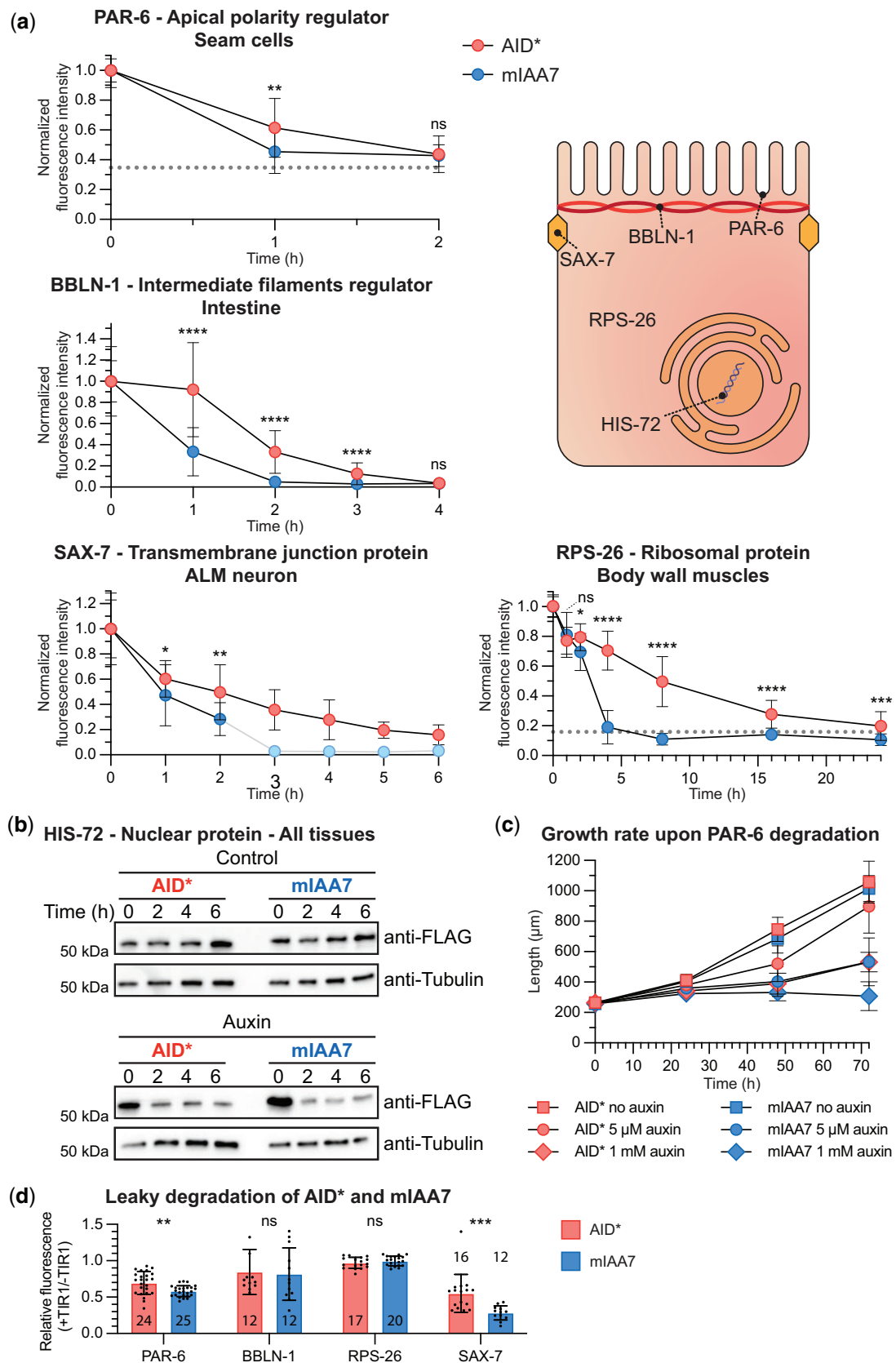


Fig. 2. The mIAA7 degron robustly increases the efficiency of AID-induced protein degradation for several proteins across multiple tissues and cellular compartments. a) Comparison between AID* and mIAA7-mediated degradation for indicated proteins and tissues. Drawing represents a generic polarized cell with the subcellular localization of the proteins investigated indicated. PAR-6 was measured at the apical domain of seam cells in L2 larvae on 5 μM auxin, BBLN-1 was measured at the apical domain in the intestine of L3 larvae treated with 50 μM auxin, SAX-7 was measured at the plasma membrane in the ALM neuron cell body of L3 larvae treated with 5 μM auxin, and RPS-26 was measured in the cytoplasm of body wall muscles of L2 larvae treated with 1 mM auxin. Values are normalized to the mean intensity levels at 0 h of auxin exposure, and each data point represents the

(continued)

The mIAA7 degron is compatible with the *C.e.*AID2 system

Recently, the AID2 system utilizing a TIR1 variant altered to fit the bulky auxin-derivative 5-Ph-IAA was adapted for *C. elegans* and shown to sharply reduce or eliminate leaky degradation while requiring low micromolar concentrations of 5-Ph-IAA (Hills-Muckey et al. 2022; Negishi et al. 2022). Given these advantages, we set out to test whether the *C.e.*AID2 system is compatible with the novel mIAA7 degron. We used CRISPR/Cas9 genome editing to introduce the F79G mutation into the TIR1 transgene in our PAR-6 and SAX-7 mIAA7 strains. Protein fluorescence levels were measured in these strains comparing animals not expressing TIR1, animals expressing TIR1[F79G] in the absence of auxin analog, and animals expressing TIR1[F79G] in the presence of 1 μ M 5-Ph-IAA. Protein levels of PAR-6 in the seam cells and SAX-7 ALM neuron cell body were not affected by the presence of TIR1[F79G], demonstrating that the mIAA7 degron does not induce leaky degradation when combined with TIR1[F79G]. Importantly, exposure to 1 μ M 5-Ph-IAA yielded complete degradation of the target proteins (Fig. 3, a and b). Thus, similar to the

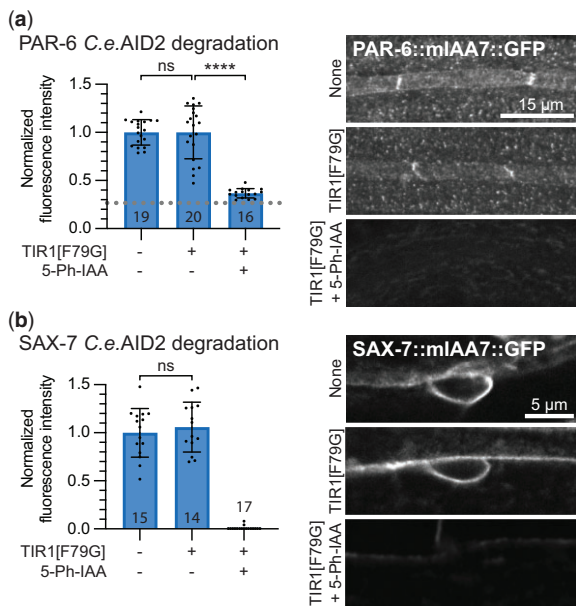


Fig. 3. The mIAA7 degron is compatible with the *C.e.*AID2 system. mIAA7-mediated degradation of PAR-6 in the seam cells (a) and of SAX-7 in the ALM neuron (b) of L2 larvae using the *C.e.*AID2 system. Values are normalized to the mean intensity levels of animals expressing the same degron-tagged proteins but not expressing TIR1 and not treated with 5-Ph-IAA (i.e. the first bar). Each data point in the graph represents a single animal. Error bars: mean \pm SD; statistical test: 1-way ANOVA with Šidák multiple testing correction; n values are indicated in or above the bars. Images shown are representative maximum intensity projections that were acquired and displayed with the same settings for comparison.

Fig. 2. Continued

average intensity for the given condition and timepoint. Due to the nature of the quantification for PAR-6 and RPS-26, the fluorescence levels did not reach zero as they did for the other targets. Nonzero baseline level values of wildtype animals are indicated, resembling a completely degraded protein pool. For SAX-7 degradation using the mIAA7 degron, exposure to auxin of 3 h or longer resulted in complete depletion and an inability to locate the ALM cell body. For these timepoints, values were plotted at 0 and no statistics were performed (light shaded dots). Error bars: mean \pm SD; Statistical test: Mann-Whitney U test; n = 9–29 animals. b) Western blots detecting HIS-72: AID*::3xFLAG and HIS-72::mIAA7::3xFLAG in synchronized control or 4 mM auxin-treated L1 larvae. An anti-alpha-tubulin loading control and protein size standard markers in kilodaltons are provided. Time in hours in control media or 4 mM auxin containing media is indicated. c) Comparison of Larval growth between AID*- and mIAA7-mediated PAR-6 degradation in the epidermis using 5 μ M and 1 mM auxin. d) Comparison of leaky degradation between AID* and mIAA7 degrons for the indicated proteins. Measurements for each protein were done as in panel A. Values are normalized to the mean intensity levels of animals expressing the same degron-tagged protein but not expressing TIR1. Each data point in the graph represents a single animal. Error bars: mean \pm SD; statistical test: Mann-Whitney U test; n values are indicated in or above the bars.

AID* and mAID degrons that were previously tested (Hills-Muckey et al. 2022; Negishi et al. 2022), the mIAA7 degron is compatible with the AID2 TIR1[F79G] variant, resulting in effective degradation at low auxin analog concentrations and no observable leaky degradation.

The use of multiple degrons can improve the efficacy of the AID system

As a final test of the efficacy of the mIAA7 degron, we tagged the ezrin/radixin/moesin ortholog ERM-1 with mIAA7. ERM-1 is highly expressed in the intestine, where it is required for microvilli formation and patterning of the lumen. The ERM-1 protein appears highly stable and shows little turnover at the apical domain (Ramalho et al. 2020; Sepers et al. 2022). Previously, we have tested both AID- and ZIF-1-mediated depletion approaches, neither of which resulted in full depletion of intestinal ERM-1 (Ramalho et al. 2020; Sepers et al. 2022). Therefore, we wanted to test if the novel mIAA7 degron could improve ERM-1 degradation. We tagged the endogenous *erm-1* locus with mCherry and mIAA7 or AID* degron coding sequences using CRISPR/Cas9 genome engineering. We then compared ERM-1 degradation in the intestine using TIR1[F79G] and 1 μ M 5-Ph-IAA, measuring fluorescence levels at the apical domain of the intestine throughout larval development in synchronized animals. Whereas the AID* degron did not yield any detectable degradation, the use of the mIAA7 degron caused significant depletion of ERM-1, again confirming that mIAA7 improves the efficacy of the AID system (Fig. 4a). However, ~76% of ERM-1 remained after 24 h and fluorescence levels did not further decrease in the following days. Thus, mIAA7-mediated degradation of ERM-1 in the intestine is still inefficient.

In yeast, it has been shown that addition of multiple degrons to a protein can improve the AID-mediated degradation rate (Kubota et al. 2013; Zhang et al. 2022). In addition, in human cell lines, the degradation rate has been shown to be affected by the localization of the degron tag (Li et al. 2019). We therefore investigated whether altering the number or position of degrons could improve ERM-1 degradation. Originally, ERM-1 was C-terminally tagged with mCherry followed by the mIAA7 degron (Fig. 4b—“C-terminal”). To test the effect of multiple degrons, we engineered similar alleles with double and triple mIAA7 degrons (Fig. 4b—“C-term 2 \times ,” “C-term 3 \times ”). To test the influence of the degron position we also generated an allele with mIAA7 located internally between the ERM-1 and mCherry coding sequences (Fig. 4b—“Internal”) and an allele combining the internal and C-terminal mIAA7 tags (Fig. 4b—“Inter + C-term”).

Synchronized animals carrying the different mIAA7 *erm-1* alleles and expressing TIR1[F79G] in the intestine were exposed to 5-Ph-IAA for 24 h and apical ERM-1 fluorescence levels were measured. Adding an additional degron to the ERM-1 C-terminus significantly improved the degradation, depleting ~3.5 times

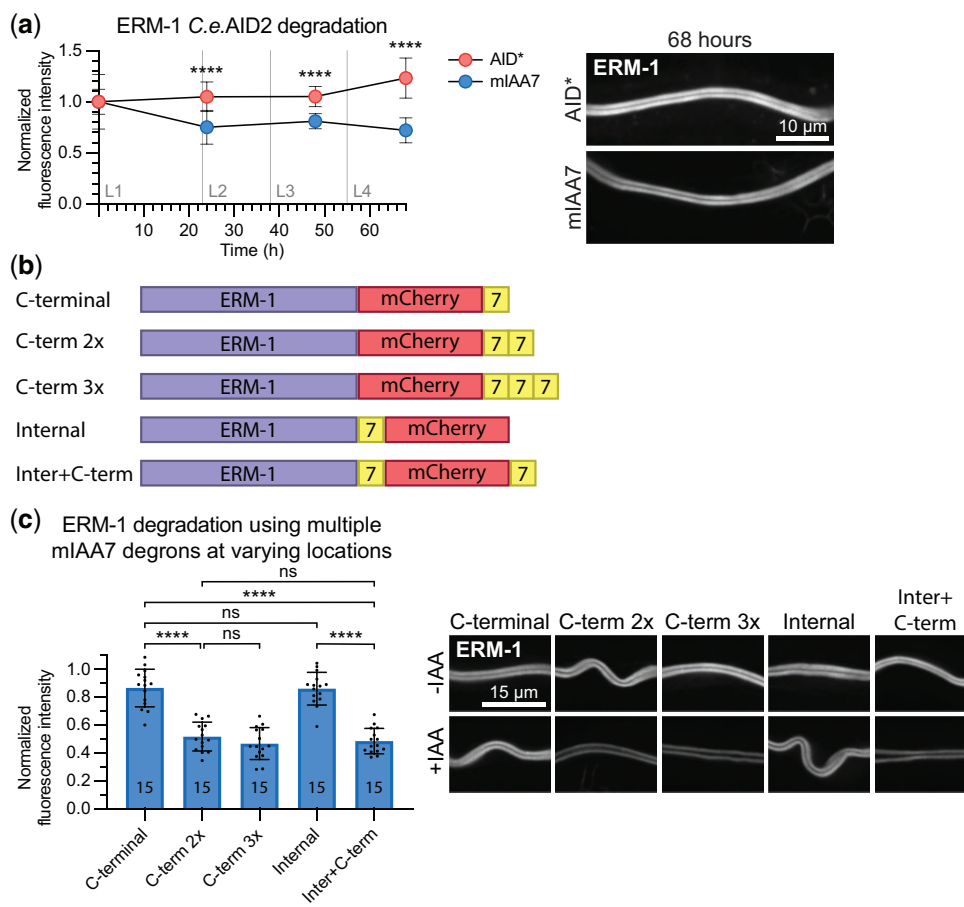


Fig. 4. Tagging ERM-1 with multiple mIAA7 degrons improves auxin-mediated degradation of intestinal ERM-1 throughout larval development using the *C.e.*AID2 system. a) Comparison between AID* and mIAA7-mediated degradation of intestinal ERM-1 using the *C.e.*AID2 system. Data points represent the mean intensity normalized to the mean intensity levels of animals with the same genotype and age that were not exposed to 5-Ph-IAA. Error bars: mean \pm SD; Statistical test: Mann-Whitney *U* test; $n = 12$ –16 animals. Images shown are representative maximum intensity projections that were acquired and displayed with the same settings for comparison. b) Schematic overview of the different ERM-1 alleles used for testing the effect of multiple degrons and degon location on auxin-mediated degradation efficiency. c) Comparison of intestinal degradation of ERM-1 tagged with 1 or multiple mIAA7 degrons at varying locations in L3 larvae using the *C.e.*AID2 system. Values are normalized to the mean intensity levels of animals with the same genotype that were not exposed to 5-Ph-IAA, and each data point represents a single animal. Images shown are representative maximum intensity projections that were acquired and displayed with the same settings for comparison. Error bars: mean \pm SD; statistical test: 1-way ANOVA with Sidák multiple testing correction; n values are indicated in the bars.

more protein than a single degon. Nevertheless, $\sim 50\%$ of ERM-1 protein remained present. Adding a third degon to the C-terminus did not result in a further increase in degradation. We did not observe a significant difference in depletion levels between ERM-1 variants with different locations of the mIAA7 tags. Both single mIAA7 tagged alleles showed similar levels of ERM-1 depletion, as did the double ERM-1 tags “C-term 2x” and “Inter + C-term.” This suggests that the positioning of the degon does not greatly alter AID-mediated degradation efficacy. In addition, when using multiple degrons in ERM-1, it is irrelevant whether they are placed in tandem or at distinct positions. In summary, AID-mediated protein degradation of ERM-1 can be further improved by using multiple degrons tags, while the position of the degrons has no significant effect on degradation efficiency.

Plasmid toolkit

To facilitate CRISPR/Cas9-mediated tagging of target proteins with the mIAA7 degon and commonly used fluorescent proteins we generated a plasmid toolkit (Supplementary Fig. 3). The plasmids encode 1 of 5 different fluorescent proteins flanked by the mIAA7 degon on either the N- or C-terminal side, and by a 12-amino acid glycine-rich linker on the opposing side. In addition,

we generated a plasmid with GFP and 3 FLAG epitope tags for detection and analysis of a target protein using an antibody. Using these plasmids to generate dsDNA repair templates allows for tagging of a protein of interest both N- and C-terminally with a choice of positioning the mIAA7 degon between the fluorescent protein and the protein of interest, or at the exposed terminus of the fluorescent protein. By designing primers with homology arms as overhangs according to established CRISPR-Cas9 protocols (Paix et al. 2015; Dokshin et al. 2018) this plasmid toolkit greatly facilitates the generation of double-stranded DNA repair templates for CRISPR/Cas9 genome engineering of fluorescently tagged AID alleles.

Discussion

The AID system is becoming increasingly popular in the *C. elegans* field due to its ability to degrade target proteins with both spatial and temporal control (Zhang et al. 2015; Ashley et al. 2021; Hills-Muckey et al. 2022; Negishi et al. 2022). However, the degradation efficiency varies between proteins, and not all proteins are depleted to the extent that expected phenotypes are observed (Patel and Hobert 2017; Serrano-Saiz et al. 2018; Duong et al. 2020; Riga

et al. 2021). Here, we demonstrated that an alternative degron sequence, termed mIAA7, improves the efficiency of degradation in *C. elegans*, as previously reported in human cell culture (Li et al. 2019).

The improvements to degradation efficiency appear to be applicable to most proteins, as we observed increased depletion efficiency for 6 proteins tested, each with different subcellular localizations and investigated in different tissue types. The only exception was the nuclear protein HIS-72, which was depleted with similar efficiency. In human cells, mIAA7 did not improve the depletion of the highly expressed nuclear proteins LMNA and LMNB1 (Li et al. 2019). However, depletion of these proteins was strongly increased when using an auxin receptor F-box protein targeted to the nucleus. A similar modification may therefore improve the depletion of nuclear proteins in *C. elegans* as well.

There are two main differences between mIAA7 and AID* that could contribute to the difference in degradation efficiency. First, mIAA7 is derived from IAA7 instead of IAA17, and hence differs in exact primary sequence. Second, the 2 degrons contain different parts of the IAA protein. While both degrons contain IAA Domain II, mIAA7 has a longer N-terminal extension and shorter C-terminal extension than AID* (Fig. 1a). A degron derived of IAA17 using the same protein region as mIAA7 resulted in a degradation speed close to mIAA7 in human cell culture (Li et al. 2019), which suggests that it is the region of the IAA protein used rather than the primary sequence that determines degradation efficiency. In support of this hypothesis, the region N-terminal to domain II was shown to be required for TIR1-mediated degradation in plants (Dreher et al. 2006; Moss et al. 2015). However, replacing the mIAA7 sequence downstream of domain II with the same region from IAA12 lowered the degradation speed, indicating that primary sequence can affect degradation efficiency as well (Niemeyer et al. 2020). One way the primary sequence could affect degradation efficiency is by providing lysine residues that can be ubiquitinated. However, the conserved KR sequence, hypothesized to be important for degradation (Dreher et al. 2006; Moss et al. 2015), is absent from the mIAA7 degron and including it did not improve degradation in human cell culture (Li et al. 2019). Moreover, all IAA7 ubiquitination sites that were found using mass spectrometry or are bioinformatically predicted are absent from the mIAA7 degron sequence (Niemeyer et al. 2020; Wang et al. 2021). Finally, IAA1 has been reported to be ubiquitinated and degraded without any lysine residues (Gilkerson et al. 2015). These data suggest that the degron itself is not ubiquitinated by the TIR1-SCF complex or that IAA proteins can be ubiquitinated in a non-canonical manner. An alternative explanation for the effects of primary sequence on degradation efficiency is offered by a recent model based on crosslinking proteomics, in which the regions flanking domain II contribute to the stability of the interaction between TIR1/Auxin Signaling F-Box (AFB) proteins, IAA proteins, and auxin (Niemeyer et al. 2020). While IAA7 showed the strongest interaction with TIR1 out of 8 IAA proteins by yeast 2-hybrid (Calderón Villalobos et al. 2012; Niemeyer et al. 2020), *Arabidopsis* alone encodes 29 IAA proteins and 6 AFBs (Liscum and Reed 2002; Parry et al. 2009; Luo et al. 2018; Morffy and Strader 2022). Therefore, even more effective IAA-AFB combinations may be discovered.

One of the drawbacks of the AID system is the potential for degradation in the absence of auxin. In our experiments, RPS-26 and BBLN-1 showed little leaky degradation with either degron, but leaky degradation for PAR-6 and SAX-7 was relatively high for AID* and was enhanced by use of the mIAA7 degron. Importantly, when combining the mIAA7 degron with the *C.e.*AID2 system that utilizes TIR1[F79G] and the auxin-derivative

5-Ph-IAA, we observed no leaky degradation of PAR-6 and SAX-7 in the absence of auxin/5-Ph-IAA. Thus, the benefits of the mIAA7 degron can be realized without the drawback of increased leaky degradation. Additional measures that users could take to address leaky degradation include reducing the expression levels of TIR1, using AFB2 instead of TIR1 (Li et al. 2019), or re-engineering the degron sequence to include the PB1 domain of Auxin Response Factor plant proteins, which was shown to reduce leaky degradation of AID degron-tagged proteins in human cell culture (Sathyan et al. 2019).

Despite the improvements in degradation kinetics conferred by the mIAA7 degron, some proteins remain refractive to full depletion. For difficult to degrade proteins, the addition of multiple degron sequence can further increase the degradation efficiency. In our hands, auxin-mediated degradation of ERM-1 was improved when tagged with two mIAA7 degrons compared to a single degron. This finding is in line with previous results in yeast, in which using multiple degrons improved degradation (Kubota et al. 2013; Zhang et al. 2022). However, in contrast to results in yeast, we did not observe a further improvement in the depletion efficiency when using three degrons. This difference may be specific to ERM-1, which associates very stably with the apical domain of intestinal cells (Ramalho et al. 2020; Sepers et al. 2022). It is possible, therefore, that a fraction of ERM-1 is not accessible to the SCF complex or the proteasome and that all accessible ERM-1 is degraded after 24 h using two degrons. Alternatively, the ubiquitination or degradation machinery may be rate limiting due to the high expression levels of ERM-1.

Interestingly, the position of the degrons did not seem to affect the degradation rate of ERM-1. Two degrons in tandem resulted in similar depletion levels as two degrons flanking the mCherry sequence on both sides. We did not test an N-terminal placement of the degron as the two predicted splice variants of ERM-1 do not share the same N-terminus, resulting in the degradation of only a subpopulation of ERM-1. Our results contrast with data from human cell culture in which degron position did influence the degradation rate for 2 proteins tested (Li et al. 2019). For the protein SEC61B degradation was higher when mIAA7 was positioned at the extreme N-terminus compared to an internal position between a fluorescent protein and SEC61B. For the protein Seipin, a C-terminal degron performed better than an N-terminal degron, and including a fluorescent protein downstream of the C-terminal degron further increased degradation efficiency. Given the low number of proteins tested in *C. elegans* and human cells, the exact influence of degron position requires further investigation. (Li et al. 2019). For the protein SEC61B degradation was higher when mIAA7 was positioned at the extreme N-terminus compared to an internal position between a fluorescent protein and SEC61B. For the protein Seipin, a C-terminal degron performed better than an N-terminal degron, and including a fluorescent protein downstream of the C-terminal degron further increased degradation efficiency. Given the low number of proteins tested in *C. elegans* and human cells, the exact influence of degron position requires further investigation.

In summary, the mIAA7 degron further extends the usability of the AID system in *C. elegans*, improving degradation efficiency while, particularly in combination with *C.e.*AID2, not affecting the steady-state level of proteins in the absence of auxin.

Data availability

All strains and plasmids are available upon request. In addition, the toolkit plasmids are available through Addgene using the

following Addgene IDs: pJJS001 = # 188324, pJJS002 = # 188325, pJJS003 = # 188326, pJJS004 = # 188327, pJJS005 = # 188328, pJJS006 = # 188329, pJJS007 = # 188330, pJJS008 = # 188331, pJJS009 = # 188332, pJJS010 = # 188333, pJJS011 = # 188334, pJJS012 = # 188335, and pJW2341 = # 186950. The authors affirm that all data necessary for confirming the conclusions of the article are present within the text or figures.

Supplemental material is available at G3 online.

Acknowledgments

We thank members of the S. van den Heuvel and M. Boxem groups for helpful discussions. We thank A. Riga for providing BOX523 and BOX857, D.J. Dolfing for providing SUR5 and SUR23, and V.C. Portegijs for providing the codon optimized wrmScarlet gBlock. We also thank Wormbase (Harris et al. 2020) and the Biology Imaging Center, Faculty of Sciences, Department of Biology, Utrecht University. Some strains were provided by the *Caenorhabditis* Genetics Center, which is funded by NIH Office of Research Infrastructure Programs (P40 OD010440). The anti-alpha tubulin 12G10 monoclonal antibody developed by J. 438 Frankel and E.M. Nelson of the University of Iowa was obtained from the Developmental Studies Hybridoma Bank, created by the NICHD of the NIH and maintained at The University of Iowa, Department of Biology, Iowa City, IA 52242.

Funding

This work was supported by the NIH/National Institute of General Medical Sciences R01 GM138701 to JDW and by the Netherlands Organization for Scientific Research (NWO) 016.VICI.170.165 grant to MB.

Author contributions

Conceptualization: JJS and MB; Formal analysis: JJS, NHMV, and JDW; Investigation: JJS, NHMV, AAV, SR, and JDW; Resources: JJS, NHMV, JMR, SR, JDW, and MB; Writing—original draft: JJS and NHMV; Writing—review and editing: SR, JDW, and MB; Visualization: JJS; Supervision: JJS, JDW, and MB; Project administration: JDW and MB; and Funding acquisition: JDW and MB.

Conflicts of interest

None declared.

Literature cited

Armenti ST, Lohmer LL, Sherwood DR, Nance J. Repurposing an endogenous degradation system for rapid and targeted depletion of *C. elegans* proteins. *Development*. 2014;141(23):4640–4647. <https://doi.org/10.1242/dev.115048>.

Ashley GE, Duong T, Levenson MT, Martinez MAQ, Johnson LC, Hibshman JD, Saeger HN, Palmisano NJ, Doonan R, Martinez-Mendez R, et al. An expanded auxin-inducible degron toolkit for *Caenorhabditis elegans*. *Genetics*. 2021;217(3):iyab006. <https://doi.org/10.1093/genetics/iyab006>.

Bhoi A, Palladino F, Fabrizio P. Auxin confers protection against ER stress in *Caenorhabditis elegans*. *Biol Open*. 2021;10:bio057992. <https://doi.org/10.1242/bio.057992>.

Bossinger O, Klebes A, Segbert C, Theres C, Knust E. Zonula adherens formation in *Caenorhabditis elegans* requires *dlg-1*, the homologue

of the *Drosophila* gene discs large. *Dev Biol*. 2001;230(1):29–42. <https://doi.org/10.1006/dbio.2000.0113>.

Brenner S. The genetics of *Caenorhabditis elegans*. *Genetics*. 1974;77(1):71–94.

Calderón Villalobos LIA, Lee S, De Oliveira C, Iveta A, Brandt W, Armitage L, Sheard LB, Tan X, Parry G, Mao H, et al. A combinatorial TIR1/AFB–Aux/IAA co-receptor system for differential sensing of auxin. *Nat Chem Biol*. 2012;8(5):477–485. <https://doi.org/10.1038/nchembio.926>.

Castiglioni VG, Pires HR, Rosas Bertolini R, Riga A, Kerver J, Boxem M. Epidermal PAR-6 and PKC-3 are essential for larval development of *C. elegans* and organize non-centrosomal microtubules. *eLife*. 2020;9:e2067. <https://doi.org/10.7554/eLife.62067>.

Cheng Z, Yi P, Wang X, Chai Y, Feng G, Yang Y, Liang X, Zhu Z, Li W, Ou G. Conditional targeted genome editing using somatically expressed TALENs in *C. elegans*. *Nat Biotechnol*. 2013;31(10):934–937. <https://doi.org/10.1038/nbt.2674>.

Cho U, Zimmerman SM, Chen L, Owen E, Kim JV, Kim SK, Wandless TJ. Rapid and tunable control of protein stability in *Caenorhabditis elegans* using a small molecule. *PLoS One*. 2013;8(8):e72393. <https://doi.org/10.1371/journal.pone.0072393>.

Davis MW, Morton JJ, Carroll D, Jorgensen EM. Gene activation using FLP recombinase in *C. elegans*. *PLoS Genet*. 2008;4(3):e1000028. <https://doi.org/10.1371/journal.pgen.1000028>.

Dickinson DJ, Pani AM, Heppert JK, Higgins CD, Goldstein B. Streamlined genome engineering with a self-excising drug selection cassette. *Genetics*. 2015;200(4):1035–1049. <https://doi.org/10.1534/genetics.115.178335>.

Dokshin GA, Ghanta KS, Piscopo KM, Mello CC. Robust genome editing with short single-stranded and long, partially single-stranded DNA donors in *Caenorhabditis elegans*. *Genetics*. 2018;210(3):781–787. <https://doi.org/10.1534/genetics.118.301532>.

Dreher KA, Brown J, Saw RE, Callis J. The *Arabidopsis* Aux/IAA protein family has diversified in degradation and auxin responsiveness. *Plant Cell*. 2006;18(3):699–714. <https://doi.org/10.1105/tpc.105.039172>.

Duong T, Rasmussen NR, Ballato E, Mote FS, Reiner DJ. The Rheb-TORC1 signaling axis functions as a developmental checkpoint. *Development*. 2020;147:dev181727. <https://doi.org/10.1242/dev.181727>.

El Mouridi S, Peng Y, Frøkjær-Jensen C. Characterizing a strong pan-muscular promoter (Pmlc-1) as a fluorescent co-injection marker to select for single-copy insertions. *MicroPubl Biol*. 2020. <https://doi.org/10.17912/micropub.biology.000302>.

Firestein BL, Rongo C. DLG-1 is a MAGUK similar to SAP97 and is required for adherens junction formation. *Mol Biol Cell*. 2001;12(11):3465–3475. <https://doi.org/10.1091/mbc.12.11.3465>.

Ghanta KS, Ishidate T, Mello CC. Microinjection for precision genome editing in *Caenorhabditis elegans*. *STAR Protoc*. 2021;2(3):100748. <https://doi.org/10.1016/j.xpro.2021.100748>.

Gibson DG, Young L, Chuang R-Y, Venter JC, Hutchison CA, Smith HO. Enzymatic assembly of DNA molecules up to several hundred kilobases. *Nat Methods*. 2009;6(5):343–345. <https://doi.org/10.1038/nmeth.1318>.

Gilkerson J, Kelley DR, Tam R, Estelle M, Callis J. Lysine residues are not required for proteasome-mediated proteolysis of the auxin/indole acetic acid protein IAA1. *Plant Physiol*. 2015;168(2):708–720. <https://doi.org/10.1104/pp.15.00402>.

Gray WM, Kepinski S, Rouse D, Leyser O, Estelle M. Auxin regulates SCFTIR1-dependent degradation of AUX/IAA proteins. *Nature*. 2001;414(6861):271–276. <https://doi.org/10.1038/35104500>.

Harris TW, Arnaboldi V, Cain S, Chan J, Chen WJ, Cho J, Davis P, Gao S, Grove CA, Kishore R, et al. WormBase: a modern model

- organism information resource. *Nucleic Acids Res.* 2020;48(D1):D762–D767. <https://doi.org/10.1093/nar/gkz920>.
- Hills-Muckey K, Martinez MAQ, Stec N, Hebbar S, Saldanha J, Medwig-Kinney TN, Moore FEQ, Ivanova M, Morao A, Ward JD, et al. An engineered, orthogonal auxin analog/AtTIR1(F79G) pairing improves both specificity and efficacy of the auxin degradation system in *Caenorhabditis elegans*. *Genetics*. 2022;220(2):iyab174. <https://doi.org/10.1093/genetics/iyab174>.
- Hoier EF, Mohler WA, Kim SK, Hajnal A. The *Caenorhabditis elegans* APC-related gene *apr-1* is required for epithelial cell migration and *Hox* gene expression. *Genes Dev.* 2000;14(7):874–886. <https://doi.org/10.1101/gad.14.7.874>.
- Housden BE, Muhar M, Gemberling M, Gersbach CA, Stainier DYR, Seydoux G, Mohr SE, Zuber J, Perrimon N. Loss-of-function genetic tools for animal models: cross-species and cross-platform differences. *Nat Rev Genet.* 2017;18(1):24–40. <https://doi.org/10.1038/nrg.2016.118>.
- Johnson LC, Vo AA, Clancy JC, Aguilera J, Levenson MT, Wohlenberg C, Rechtsteiner A, Ragle J, Ward JD. NHR-23 activity is necessary for developmental progression and apical extracellular matrix structure and function. *bioRxiv*. 2022. <https://doi.org/10.1101/2021.10.27.465992>.
- Köppen M, Simske JS, Sims PA, Firestein BL, Hall DH, Radice AD, Rongo C, Hardin JD. Cooperative regulation of AJM-1 controls junctional integrity in *Caenorhabditis elegans* epithelia. *Nat Cell Biol.* 2001;3(11):983–991. <https://doi.org/10.1038/ncb1101-983>.
- Kroll JR, Rimmelzwaal S, Boxem M. CeLINC, a fluorescence-based protein-protein interaction assay in *Caenorhabditis elegans*. *Genetics*. 2021;219(4):iyab163. <https://doi.org/10.1093/genetics/iyab163>.
- Kubota T, Nishimura K, Kanemaki MT, Donaldson AD. The Elg1 replication factor C-like complex functions in PCNA unloading during DNA replication. *Mol Cell.* 2013;50(2):273–280. <https://doi.org/10.1016/j.molcel.2013.02.012>.
- Li S, Prasanna X, Salo VT, Vattulainen I, Ikonen E. An efficient auxin-inducible degron system with low basal degradation in human cells. *Nat Methods.* 2019;16(9):866–869. <https://doi.org/10.1038/s41592-019-0512-x>.
- Liscum E, Reed JW. Genetics of Aux/IAA and ARF action in plant growth and development. *Plant Mol Biol.* 2002;49(3–4):387–400. https://doi.org/10.1007/978-94-010-0377-3_10.
- Loose JA, Ghazi A. Auxin treatment increases lifespan in *Caenorhabditis elegans*. *Biol Open.* 2021;10:bio058703. <https://doi.org/10.1242/bio.058703>.
- Luo J, Zhou J-J, Zhang J-Z. Aux/IAA gene family in plants: molecular structure, regulation, and function. *Int J Mol Sci.* 2018;19(1):259. <https://doi.org/10.3390/ijms19010259>.
- Martinez MAQ, Kinney BA, Medwig-Kinney TN, Ashley G, Ragle JM, Johnson L, Aguilera J, Hammell CM, Ward JD, Matus DQ. Rapid degradation of *Caenorhabditis elegans* proteins at single-cell resolution with a synthetic auxin. *G3 (Bethesda)*. 2020;10(1):267–280. <https://doi.org/10.1534/g3.119.400781>.
- McMahon L, Legouis R, Vonesch JL, Labouesse M. Assembly of *C. elegans* apical junctions involves positioning and compaction by LET-413 and protein aggregation by the MAGUK protein DLG-1. *J Cell Sci.* 2001;114(Pt 12):2265–2277. <https://doi.org/10.1242/jcs.114.12.2265>.
- Mello CC, Kramer JM, Stinchcomb D, Ambros V. Efficient gene transfer in *C. elegans*: extrachromosomal maintenance and integration of transforming sequences. *EMBO J.* 1991;10(12):3959–3970.
- Mendoza-Ochoa GI, Barrass JD, Terlouw BR, Maudlin IE, de Lucas S, Sani E, Aslanzadeh V, Reid JAE, Beggs JD. A fast and tuneable auxin-inducible degron for depletion of target proteins in budding yeast. *Yeast.* 2019;36(1):75–81. <https://doi.org/10.1002/yea.3362>.
- Morawska M, Ulrich HD. An expanded tool kit for the auxin-inducible degron system in budding yeast. *Yeast.* 2013;30(9):341–351. <https://doi.org/10.1002/yea.2967>.
- Morffy N, Strader LC. Structural aspects of auxin signaling. *Cold Spring Harb Perspect Biol.* 2022;14(1):a039883. <https://doi.org/10.1101/cshperspect.a039883>.
- Moss BL, Mao H, Guseman JM, Hinds TR, Hellmuth A, Kovenock M, Noorassa A, Lanctot A, Villalobos LIAC, Zheng N, et al. Rate motifs tune auxin/indole-3-acetic acid degradation dynamics. *Plant Physiol.* 2015;169(1):803–813. <https://doi.org/10.1104/pp.15.00587>.
- Muñoz-Jiménez C, Ayuso C, Dobrzynska A, Torres-Mendéz A, Ruiz P, de la C, Askjaer P. An efficient FLP-based toolkit for spatiotemporal control of gene expression in *Caenorhabditis elegans*. *Genetics*. 2017;206(4):1763–1778. <https://doi.org/10.1534/genetics.117.201012>.
- Nance J, Frøkjær-Jensen C. The *Caenorhabditis elegans* transgenic toolbox. *Genetics*. 2019;212(4):959–990. <https://doi.org/10.1534/genetics.119.301506>.
- Natsume T, Kiyomitsu T, Saga Y, Kanemaki MT. Rapid protein depletion in human cells by auxin-inducible degron tagging with short homology donors. *Cell Rep.* 2016;15(1):210–218. <https://doi.org/10.1016/j.celrep.2016.03.001>.
- Negishi T, Asakawa M, Kanemaki M, Sawa H. Modified auxin improves the auxin-inducible degradation (AID) system for laid *C. elegans* embryos. *MicroPubl Biol.* 2019;2019(10.17912): <https://doi.org/10.17912/micropub.biology.000190>.
- Negishi T, Kitagawa S, Horii N, Tanaka Y, Haruta N, Sugimoto A, Sawa H, Hayashi K, Harata M, Kanemaki MT. The auxin-inducible degron 2 (AID2) system enables controlled protein knockdown during embryogenesis and development in *Caenorhabditis elegans*. *Genetics*. 2022;220(2):iyab218. <https://doi.org/10.1093/genetics/iyab218>.
- Niemeyer M, Moreno Castillo E, Ihling CH, Iacobucci C, Wilde V, Hellmuth A, Hoehenwarter W, Samodelov SL, Zurbriggen MD, Kastiris PL, et al. Flexibility of intrinsically disordered degrons in AUX/IAA proteins reinforces auxin co-receptor assemblies. *Nat Commun.* 2020;11(1):2277. <https://doi.org/10.1038/s41467-020-16147-2>.
- Nishimura K, Fukagawa T, Takisawa H, Kakimoto T, Kanemaki M. An auxin-based degron system for the rapid depletion of proteins in nonplant cells. *Nat Methods.* 2009;6(12):917–922. <https://doi.org/10.1038/nmeth.1401>.
- Paix A, Folkmann A, Rasoloson D, Seydoux G. High efficiency, homology-directed genome editing in *Caenorhabditis elegans* using CRISPR-Cas9 ribonucleoprotein complexes. *Genetics*. 2015;201(1):47–54. <https://doi.org/10.1534/genetics.115.179382>.
- Parry G, Calderon-Villalobos LI, Prigge M, Peret B, Dharmasiri S, Itoh H, Lechner E, Gray WM, Bennett M, Estelle M. Complex regulation of the TIR1/AFB family of auxin receptors. *Proc Natl Acad Sci U S A.* 2009;106(52):22540–22545. <https://doi.org/10.1073/pnas.0911967106>.
- Patel T, Hobert O. Coordinated control of terminal differentiation and restriction of cellular plasticity. *eLife.* 2017;6:e24100. <https://doi.org/10.7554/eLife.24100>.
- Qadota H, Inoue M, Hikita T, Köppen M, Hardin JD, Amano M, Moerman DG, Kaibuchi K. Establishment of a tissue-specific RNAi system in *C. elegans*. *Gene.* 2007;400(1–2):166–173. <https://doi.org/10.1016/j.gene.2007.06.020>.
- Ramalho JJ, Sepers JJ, Nicolle O, Schmidt R, Cravo J, Michaux G, Boxem M. C-terminal phosphorylation modulates ERM-1

- localization and dynamics to control cortical actin organization and support lumen formation during *Caenorhabditis elegans* development. *Development*. 2020;147: <https://doi.org/10.1242/dev.188011>.
- Ramos JA, Zenser N, Leyser O, Callis J. Rapid degradation of auxin/indoleacetic acid proteins requires conserved amino acids of domain II and is proteasome dependent. *Plant Cell*. 2001;13(10):2349–2360. <https://doi.org/10.1105/tpc.010244>.
- Rommelzwaal S, Geisler F, Stucchi R, van der Horst S, Pasolli M, Kroll JR, Jarosinska OD, Akhmanova A, Richardson CA, Altelaar M, et al. BBLN-1 is essential for intermediate filament organization and apical membrane morphology. *Curr Biol*. 2021;31(11):2334–2346.e9. <https://doi.org/10.1016/j.cub.2021.03.069>.
- Riga A, Cravo J, Schmidt R, Pires HR, Castiglioni VG, Heuvel S, van den Boxem M. *Caenorhabditis elegans* LET-413 Scribble is essential in the epidermis for growth, viability, and directional outgrowth of epithelial seam cells. *PLoS Genet*. 2021;17(10):e1009856. <https://doi.org/10.1371/journal.pgen.1009856>.
- Ruijtenberg S, van den Heuvel S. G1/S inhibitors and the SWI/SNF complex control cell-cycle exit during muscle differentiation. *Cell*. 2015;162(2):300–313. <https://doi.org/10.1016/j.cell.2015.06.013>.
- Sallee MD, Pickett MA, Feldman JL. Apical PAR complex proteins protect against programmed epithelial assaults to create a continuous and functional intestinal lumen. *eLife*. 2021;10:e64437. <https://doi.org/10.7554/eLife.64437>.
- Sathyan KM, McKenna BD, Anderson WD, Duarte FM, Core L, Guertin MJ. An improved auxin-inducible degron system preserves native protein levels and enables rapid and specific protein depletion. *Genes Dev*. 2019;33(19–20):1441–1455. <https://doi.org/10.1101/gad.328237.119>.
- Schiksnis EC, Nicholson AL, Modena MS, Pule MN, Arribere JA, Pasquinelli AE. Auxin-independent depletion of degron-tagged proteins by TIR1. *MicroPubl Biol*. 2020. <https://doi.org/10.17912/micropub.biology.000213>.
- Schindelin J, Arganda-Carreras I, Frise E, Kaynig V, Longair M, Pietzsch T, Preibisch S, Rueden C, Saalfeld S, Schmid B, et al. Fiji: an open-source platform for biological-image analysis. *Nat Methods*. 2012;9(7):676–682. <https://doi.org/10.1038/nmeth.2019>.
- Schwartz ML, Jorgensen EM. SapTrap, a toolkit for high-throughput CRISPR/Cas9 gene modification in *Caenorhabditis elegans*. *Genetics*. 2016;202(4):1277–1288. <https://doi.org/10.1534/genetics.115.184275>.
- Sepers JJ, Ramalho JJ, Kroll JR, Schmidt R, Boxem M. ERM-1 phosphorylation and NRFL-1 redundantly control lumen formation in the *C. elegans* intestine. *Front Cell Dev Biol*. 2022;10:769862.
- Serrano-Saiz E, Leyva-Díaz E, De La Cruz E, Hobert O. BRN3-type POU homeobox genes maintain the identity of mature postmitotic neurons in nematodes and mice. *Curr Biol*. 2018;28(17):2813–2823.e2. <https://doi.org/10.1016/j.cub.2018.06.045>.
- Shen Z, Zhang X, Chai Y, Zhu Z, Yi P, Feng G, Li W, Ou G. Conditional knockouts generated by engineered CRISPR-Cas9 endonuclease reveal the roles of coronin in *C. elegans* neural development. *Dev Cell*. 2014;30(5):625–636. <https://doi.org/10.1016/j.devcel.2014.07.017>.
- Venz R, Pecek T, Katic I, Ciosk R, Ewald CY. End-of-life targeted degradation of DAF-2 insulin/IGF-1 receptor promotes longevity free from growth-related pathologies. *eLife*. 2021;10:e71335. <https://doi.org/10.7554/eLife.71335>.
- Virtanen P, Gommers R, Oliphant TE, Haberland M, Reddy T, Cournapeau D, Burovski E, Peterson P, Weckesser W, Bright J, et al; SciPy 1.0 Contributors. SciPy 1.0: fundamental algorithms for scientific computing in Python. *Nat Methods*. 2020;17(3):261–272. <https://doi.org/10.1038/s41592-019-0686-2>.
- Vo AA, Levenson MT, Ragle JM, Ward JD. Efficient generation of a single-copy *eft-3p::TIR1::F2A::BFP::AID::NLS* allele in the *C. elegans* *ttT5605* insertion site through recombination-mediated cassette exchange. *MicroPubl Biol*. 2021. <https://doi.org/10.17912/micropub.biology.000425>.
- Wang S, Tang NH, Lara-Gonzalez P, Zhao Z, Cheerambathur DK, Prevo B, Chisholm AD, Desai A, Oegema K. A toolkit for GFP-mediated tissue-specific protein degradation in *C. elegans*. *Development*. 2017;144(14):2694–2701. <https://doi.org/10.1242/dev.150094>.
- Wang X, Yan R, Chen Y-Z, Wang Y. Computational identification of ubiquitination sites in *Arabidopsis thaliana* using convolutional neural networks. *Plant Mol Biol*. 2021;105(6):601–610. <https://doi.org/10.1007/s11103-020-01112-w>.
- Wu Q, Ploegh HL, Truttmann MC. Hepta-mutant *Staphylococcus aureus* Sortase A (SrtA7m) as a tool for in vivo protein labeling in *Caenorhabditis elegans*. *ACS Chem Biol*. 2017;12(3):664–673. <https://doi.org/10.1021/acscchembio.6b00998>.
- Yesbolatova A, Natsume T, Hayashi K, Kanemaki MT. Generation of conditional auxin-inducible degron (AID) cells and tight control of degron-fused proteins using the degradation inhibitor auxinole. *Methods*. 2019;164–165:73–80. <https://doi.org/10.1016/j.ymeth.2019.04.010>.
- Yesbolatova A, Saito Y, Kitamoto N, Makino-Itou H, Ajima R, Nakano R, Nakaoka H, Fukui K, Gamo K, Tominari Y, et al. The auxin-inducible degron 2 technology provides sharp degradation control in yeast, mammalian cells, and mice. *Nat Commun*. 2020;11(1):5701. <https://doi.org/10.1038/s41467-020-19532-z>.
- Zhang L, Ward JD, Cheng Z, Dernburg AF. The auxin-inducible degradation (AID) system enables versatile conditional protein depletion in *C. elegans*. *Dev*. 2015;142:4374–4384. <https://doi.org/10.1242/dev.129635>.
- Zhang X-R, Zhao L, Suo F, Gao Y, Wu Q, Qi X, Du L-L. An improved auxin-inducible degron system for fission yeast. *G3*. 2022;12:jkab393. <https://doi.org/10.1093/g3journal/jkab393>.